

Author's Accepted Manuscript

The cold-rolling behaviour of AZ31 tubes
for fabrication of biodegradable stents

Yaowu Zhang, Damon Kent, Gui Wang,
David StJohn, Matthew S. Dargusch



www.elsevier.com/locate/jmbbm

PII: S1751-6161(14)00232-X
DOI: <http://dx.doi.org/10.1016/j.jmbbm.2014.07.026>
Reference: JMBBM1218

To appear in: *Journal of the Mechanical Behavior of Biomedical Materials*

Received date: 27 February 2014
Revised date: 23 July 2014
Accepted date:
27 July 2014

Cite this article as: Yaowu Zhang, Damon Kent, Gui Wang, David StJohn, Matthew S. Dargusch, The cold-rolling behaviour of AZ31 tubes for fabrication of biodegradable stents, *Journal of the Mechanical Behavior of Biomedical Materials*, <http://dx.doi.org/10.1016/j.jmbbm.2014.07.026>

This is a PDF file of an unedited manuscript that has been accepted for publication. As a service to our customers we are providing this early version of the manuscript. The manuscript will undergo copyediting, typesetting, and review of the resulting galley proof before it is published in its final citable form. Please note that during the production process errors may be discovered which could affect the content, and all legal disclaimers that apply to the journal pertain.

The cold-rolling behaviour of AZ31 tubes for fabrication of biodegradable stents

Yaowu Zhang*, Damon Kent, Gui Wang, David StJohn and Matthew S Dargusch

Queensland Centre for Advanced Materials Processing and Manufacturing (AMPAM),
School of Mechanical and Mining Engineering, The University of Queensland, Brisbane, QLD 4072, Australia

* *Corresponding author.*

E-mail address: y.zhang20@uq.edu.au; Phone: +61414653009

Abstract

Mg alloys are receiving considerable attention for biomedical stents due to their combination of good mechanical properties and high biodegradability. Cold rolling is necessary to process Mg alloy tubes before final drawing and fabrication of the magnesium stents. In this paper, cold-rolled tubes were subjected to a cross-sectional reduction rate (ε) of up to 19.7%, and were further processed at various ratios of wall-thickness to diameter reduction (Q) from 0 to 2.24 with a constant ε of 19.7%. The results show that the cold-rolled tubes exhibited a rise in ultimate tensile strength (UTS), yield strength (YS), and a reduction in elongation as ε increased from 5.5% to 19.7%. UTS, YS and elongation decreased when Q was increased from 0 to 2.24. Mechanical twinning was observed and analysed. Extension twins increased with increasing ε and were almost saturated at an ε of 16.5%. Extension twins play an important role in determining the evolution of mechanical behaviour in the case of increasing ε , whilst contraction/double twins and secondary extension twins have a large effect on mechanical behaviour in the case of varying Q . The results indicate that the proportions and types of twins play a major role in determining the mechanical behaviour of the AZ31 tubes.

Keywords: AZ31 tubes; processing; cold rolling; mechanical behaviour; twinning

1. Introduction

Biodegradable magnesium stents are capable of providing good mechanical properties and can achieve properties similar to conventional stents. However, biodegradable magnesium stents are able to temporarily open the blood vessels until they remodel and then can be absorbed into the body reducing the likelihood of long-term complications or risks (Erbel et al.; Hanada, Matsuzaki, Huang, & Chino, 2013). Several magnesium alloys, such as AE21 (2 wt.% Al and 1wt.% rare earth elements) and WE43 (4 wt.% Y and 3 wt.% rare earth elements), have been investigated in recent years (Heublein et al., 2003). Also, another alloy, Mg-Li-Zn, has been patented for use in biodegradable implants (Hermawan, Dubé, & Mantovani, 2010). Although there is still discussion on the addition of aluminium to bio-materials (Farrar, Blair, Altmann, & Welch, 1990; Phillipson, 1988), Mg-Al-Zn alloys are widely used for research on the processing of biomedical Mg alloys as they are commonly available commercial alloys (Hu et al., 2011; Zeng, Hu, Guan, Cui, & Han). AZ31 was used in this

paper to investigate the cold-rolling behaviour of magnesium tubes.

The hexagonal close-packed (HCP) structure of magnesium alloys is associated with poor formability and restricts plastic deformation at room temperature (Chen & Huang, 2003; L.-f. Yang, Mori, & Tsuji, 2008). Manufacture of Mg alloy tubes traditionally requires processing at elevated temperatures. However this is not suitable for fabrication of small-dimension magnesium tubes, because grain growth at elevated temperatures negatively impacts the mechanical properties and cannot be improved during consequent drawing processes (Chao, Sun, & Wang, 2011; X. Yang, Okabe, Miura, & Sakai, 2012). Therefore, cold rolling is a necessary process during the manufacture of the small-dimension magnesium tubes (Barnett, Nave, & Bettles, 2004). The two main parameters during cold rolling, ε and Q , are as defined below (Tenckhoff, 1988):

$$\varepsilon = \frac{A_1}{A_0} = \frac{t_1 \times D_1}{t_0 \times D_0} \quad (1)$$

$$Q = \frac{t_1}{D_1} = \frac{t_0}{D_0} \times \quad (2)$$

Where, A_0 and A_1 are the initial and final cross-sectional area; t_0 and t_1 are the initial and final wall thickness; D_0 and D_1 are the initial and final outside diameter (OD).

ε is defined as the amount of deformation on the cross section of the tubes and is an indicator of the change of cross-sectional size. Q is exclusive to tubes as compared with parameters used to describe the rolling of sheets. As Q increases, the ratio of wall-thickness to perimeter decreases and the tubes become thinner. Q , therefore, indicates the change in cross-sectional shape. No elongation occurs as Q changes. In the present paper, either ε or Q was held constant while the other parameter was changed during cold rolling in order to investigate their effects on the mechanical properties.

It is well known that in order to understand the deformation behaviour of Mg alloys during cold rolling two types of deformation modes, slip and twinning, need to be considered (Barnett, Nave, et al., 2004; Jiang, Jonas, Luo, Sachdev, & Godet, 2007). Strain along the c-axis can be accommodated by $\langle c + a \rangle$ slip and twinning. However, Mg alloys exhibit a strong preference for mechanical twinning because the twinning has a lower threshold stress than $\langle c + a \rangle$ slip [1-4](L. Jiang et al., 2007). Therefore, twinning plays a vital role during deformation (Liu, Jonas, Li, & Zhu, 2013). It is well known that there are typically two types of deformation twins which form in Mg; one type are $\{10\bar{1}2\}$ extension twins and the other are $\{10\bar{1}1\}$ contraction twins (Yoo, 1981). Extension twins are formed when there is an extension strain component parallel to the c-axis which is generated at the onset of plastic deformation and contributes to strain (Ball & Prangnell, 1994; Gharghoury, Weatherly, Embury, & Root, 1999; Wang & Huang, 2007). Contraction twins are generated when there is a contraction strain component parallel to the c-axis at larger levels of deformation in order to relax the stress concentration (Huber & Hatherly, 1980; Koike, 2005). As well as the two types of primary twins, secondary twinning, called double twins, can be activated within the reoriented primary twins. The extension and contraction twins are associated with the mechanical anisotropy of Mg alloys (Ball & Prangnell, 1994; Gharghoury et al., 1999; Wang & Huang, 2007). Deformation twinning may

contribute to a radical reorientation of the volume fraction of the grains that have twinned, which leads to texture modification. Conversely, during cold-rolling the activation of extension and contraction twins during plastic deformation greatly depends on the texture (Bohlen et al., 2006; Jonas et al., 2011; Meza-García et al., 2007). Twinning activity can be investigated in order to explain the evolution of mechanical behaviour of Mg tubes during cold-rolling. Liu et al. (Liu et al., 2013; Myshlyayev, McQueen, Mwembela, & Konopleva, 2002) studied the relationship between texture and deformation mode and concluded that the shape of the flow curve was determined by the type of twinning that occurs and by when the twins were activated. Variations in the strain hardening behaviour can be attributed to the influence of mechanical twinning. Knezevic et al. (Knezevic et al., 2010) reported that mechanical twins in AZ31 affected strain hardening and the main contribution to hardening comes from texture hardening. Rohatgi et al. (Rohatgi, Vecchio, & Gray, 2001) considered that the reason that twinning retards the decrease in strain hardening rate lies in the effective grain refinement that results from twinning. However, Barnett (Barnett, 2001) provided another explanation; that reorientation of the c-axes by almost 90° has a more significant effect on the strain hardening produced by twinning with c-axis extension. Jiang, et al. (Lan Jiang et al., 2007) conducted a study to determine the twinning modes and texture development under different strain paths. Their view was in accordance with that of Barnett that the effect of mechanical twinning and corresponding texture development on the flow stress is more significant than the effects of grain size. Thus, twinning development has been investigated in the present paper in order to explore the underlying mechanism of how the two cold-rolling parameters, ϵ and Q , act in determining mechanical properties of the AZ31 Mg tubes.

The cold rolling behaviour of Mg alloys has been investigated in recent years (Styczynski et al., 2004; L.-f. Yang et al., 2008). However, most studies have focused on magnesium sheets. Little research has been conducted on the fabrication of magnesium tubes, especially for mini-tubes. In this paper, the mechanical properties of magnesium mini-tubes was examined, and twinning activity was investigated in regards to the morphology and orientation of twins formed during cold rolling in order to develop an understanding of the cold-rolling behaviour of Mg alloy mini-tubes.

2. Experimental Methods

AZ31 alloy ingot was cast with a diameter of 350mm. Surface oxides were removed by turning. It was then heated to 400°C and extruded with an extrusion ratio of 42:1. The final extruded tubes had outside diameter of 7.9mm and wall thickness of 0.9mm. The chemical composition of the final extruded tubes, determined by the wet analysis method, is shown in Table 1. A mill with 3 rollers (LD-8) was used to cold roll the extruded AZ31 tubes into a series of final dimensions as shown in Table 2.

The effect of the two cold rolling parameters, ϵ and Q , has been investigated with ϵ held constant at approximately 19%, while the value of Q was varied from 0 to 2.24. Similarly, ϵ was increased from 5.5% to 19.7% while Q was held constant at 1.37. Note that the E4/Q3 group was prepared as the benchmark condition, which was cold-rolled with an ϵ of 19.7% and a Q of 1.37.

Uniaxial tensile tests were performed on all of the cold-rolled Mg tubes. Tensile specimens with nominal gauge dimensions of 25mm (length) \times 3mm (width) were taken from the tubes with their axis aligned along the Elongation direction (ED) by wire-electrode cutting (Fig. 1). In order to avoid the influence of minor notches on the machining surfaces, polishing was conducted before the tensile tests. To ensure repeatability of the results, three tensile specimens were tested for each set of conditions and the average value was then used in the results. Tensile tests were conducted on an Instron-4505 universal testing machine. A contact extensometer was used to measure the strain. As the mechanical behaviour of cold rolling and the corresponding twinning activity were of interest, tests were conducted at ambient temperatures and at a loading rate of 0.001 s⁻¹.

The surfaces examined by SEM were perpendicular to the tangential direction (TD) and polished using 6 μ m, 3 μ m, 1 μ m diamond paste and 0.02 μ m colloidal silica. Sample were then etched in a solution of 5g picric acid, 5ml acetic acid, 80ml ethanol and 10ml water for 20 s to 30 s. The microstructure was observed using a JEOL JSM-6460 scanning electron microscope. The statistical results of average grain size were obtained by the average grain intercept method using SEM images based on ASTM standard E112-13 (ASTM, 2013). For the EBSD samples, mechanical polishing was followed by a final 2-4 s etch using a solution of 5ml nitric acid, 5ml hydrofluoric acid and 90ml distilled water to improve the quality of the electron backscatter diffraction patterns (EBSP). The EBSD data were collected using an EBSD camera attached to a JEOL JSM-7001F Scanning Electron Microscope at a voltage of 25 kV. The pole figures (PFs) were obtained from post treatments using the HKL® Channel 5 software.

3. Results

3.1. Mechanical behaviour

The true stress-true strain curves for specimens processed with ϵ from 5.5% to 19.7% with a constant Q of 1.37 are presented in Fig. 2 (a). The nominal true stress was calculated based on the applied load and the strain, assuming constant volume and uniform deformation. As seen in Fig. 2 (a), all the true stress-true strain curves have a power-law type strain hardening region. With the increase of ϵ , the flow curves exhibit a distinct yield point increasing from 211MPa (ϵ of 5.5%) to 316MPa (ϵ of 19.7%). The rate of strain hardening decreased with the increase of ϵ . When the ϵ was 5.5% and 11.1%, obvious strain hardening occurs following yield. In comparison, when ϵ was increased to 16.5% and 19.7%, post-UTS regions were found to be relatively short and indicated no obvious strain hardening. Thus, the strain hardening behaviour tends to decrease with an increase in ϵ . As shown in Fig. 2 (b), the increase in ϵ results in a decrease in elongation and an increase in the ultimate tensile strength

(UTS) and yield strength (YS), which indicates fairly conventional evolution of the UTS, YS and elongation during cold working.

The true stress-true strain curves for specimens processed with Q from 0 to 2.24 and a constant ε of 19% (Fig. 3 (a)) show that yielding of the four flow curves occurred at a similar true strain of around 0.7%. The rate of flow hardening had a propensity to decrease with an increase of Q from 0 to 1.37, as did the UTS, which dropped from 369MPa to 277MPa. The UTS and YS declined with an increase in Q as shown in Fig. 3 (a). Elongation decreased from 1.55% to 0.41% showing the same trend as that of UTS and YS. This indicates that both the strength and elongation are superior in this group of specimens when the Q is at its lowest values. This does not fit the conventional relationship in that the elongation would typically be expected to increase in conjunction with reductions in the strength.

In view of the fact that the E4/Q3 group had the highest UTS and YS in the case of increasing ε , further increases in the UTS and YS (increased by 13.5%) were achieved when Q was reduced. On the other hand, elongation doubled as Q decreased from 0.53 to 0, while it remained at the same level when Q was more than 0.53. Therefore, lower Q values are beneficial to both strength and ductility.

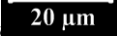
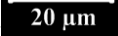
3.2. Evolution of the microstructure

The distribution of texture within extruded AZ31 tubes and rolled AZ31 sheets has been widely reported in previous literature (Barnett, Nave, et al., 2004; Chino, Hoshika, Lee, & Mabuchi, 2006; Guan, Tang, Jiang, & Chu, 2009). The grain orientations within the extruded AZ31 tubes were divided into two groups; one with their c-axis approximately parallel to the RD, called the RD component, and the other with their c-axis parallel to the TD are called the TD component (L. Jiang et al., 2007). As ε was introduced during cold-rolling, the ED component was activated due to the resolved stress in this direction (Fig. 4). It is analogous to the transverse direction in the deformation of sheets. Therefore, texture in the ED will be considered in the following analysis. According to previous literature, the morphology of well-developed $\{10\bar{1}2\}$ extension twins, are irregular, chunky and coarse (L. Jiang et al., 2007), which is quite unlike that of $\{10\bar{1}1\}$ contraction twins and double twins which are typically thin, straight and long (Koike & Ohyama, 2005; L. Zhang et al., 2013). Contraction twins which form in magnesium alloys frequently appear as the $\{10\bar{1}1\}$ - $\{10\bar{1}2\}$ double twinned structure, and they have similar morphologies and effects on the mechanical behaviour (Chino, Kimura, & Mabuchi, 2008). For a given imposed displacement along the planes of maximum shear stress, extension twins only produce small amounts of shear per unit volume and therefore a relatively large volume fraction of extension twins is required to accommodate the strain. Conversely, contraction twins produce large amounts of shear per unit volume and therefore much smaller volume fractions are produced. This explanation was originally proposed for Zr [28] and Jiang et al. (L. Jiang et al., 2007) further applied that explanation to magnesium alloys. Because there are substantial differences in the morphology of the twins, it is possible to distinguish the different types of mechanical twins from the microstructure.

Fig. 5 (a) - (c) illustrates the microstructures corresponding to increasing ε with a constant Q of 1.37. All the optical micrographs presented here are perpendicular to the TD. It shows almost equiaxed

grains for the four sets of conditions. This was consistent with the report published by Ion and co-workers (Ion, Humphreys, & White, 1982): the grain size was homogeneous for AZ31 specimens deformed at strains of up to 25%. Twinning was observed to occur even during the initial stages at an ϵ of 5.5%. Twins can be also observed within grains for all specimens. Table 3 shows the statistical results for the average grain size obtained by the average grain intercept method based on ASTM Standard E112-13 (ASTM, 2013) using Image J software on SEM images. The average grain sizes do not experience a substantial change. For this reason the grain size is not considered to be a factor in further analysis relating to the mechanical behaviours.

All of the samples in the present paper are considered to have grains which were reoriented by twinning activities, because a small amount of strain ($\sim 3\%$) on tubes induces deformation twins (Al-Samman, Molodov, Molodov, Gottstein, & Suwas, 2012; Barnett, 2007; L. Zhang et al., 2013). Valle et al. (del Valle, Carreño, & Ruano, 2006) reported that the volume fraction of twins increased with increase in strain from 5% to 15%, which is in accordance with Fig. 5 (a) - (c). The fraction volume of twins increased dramatically with an increase in ϵ , which indicates that a large amount of twins were activated during cold rolling. Fig. 5 (c) shows almost all grains contained deformation twins at an ϵ of 19.7%. It is noted that some of the twins within a particular grain were essentially parallel (see white arrows in Fig. 5 (c)). These twins were $\{10\bar{1}1\}$ contraction twins or double twins. The morphology of the extension twins had a tendency to be thick. The characteristic lenticular morphology (see black arrows in Fig. 5 (a)) was also observed, as reported by Ion et al. (Ion et al., 1982). Sideways growth of the twins occurred with increasing ϵ . In Fig. 5 (b) and (c) some of the extension twins have grown and developed into a thick rodlike morphology.

Fig. 5 (d) - (f) shows the evolution of microstructure of AZ31 specimens as Q increased from 0 to 2.37 with a constant ϵ of approximately . Equiaxed grains remained with . Grain sizes, therefore, remained constant while Q increased. In comparison with Fig. 5 (c), the volume fraction of twins remained at the condition of almost saturation. However, the proportion of contraction and double twins increased with an increase in Q (see blue arrows in Fig. 5 (e) and (f)).

It is noticed that there are two types of grains with different contrast, light-coloured and dark-coloured (Fig. 5 (a) - (c)). The basal plane of a certain grain is parallel to the observation surface, grains are light-coloured, whilst grains perpendicular to the observation surface appear to be dark-coloured (L. Zhang et al., 2013). Therefore, grains in the TD orientation should be light-coloured, and dark-coloured grains are considered to be in the RD or ED. In Fig. 5 (c), the fraction of twins appears to be low because many of the grains have been entirely consumed by well-developed extension twinning. The intersection of twins can occasionally be observed for high levels of ϵ (Fig. 5 (e) and (f)).

In order to obtain the orientation of grains and identify the twinning, EBSD serial analyses was performed (Fig. 6). The data around twins had low indexing rate due to the lattice distortion of magnesium under cold rolling conditions. However, the type of twins can be identified by their

characteristic reorientation angles (87° , 56° and 38° for extension, contraction and double twins, respectively) (Zhang, Rauch, & Véron, 2013). The observed surface is perpendicular to RD. Therefore, $\langle 0001 \rangle$ in Fig. 6 is parallel to RD. Fig. 7 is a schematic showing how to identify the different types of twins were identified. Extension twins were observed in most grains, whilst contraction and double twins can only be identified in grains with their c -axis not aligned along the $\langle 0001 \rangle$ direction. Fig. 6 (a) and (b) are from N08 and N03, where ε was increased from 5.5% to 19.7% with a Q of 1.37. The volume fraction of extension twins increased dramatically. Fig. 6 (c) and (d) are from N02 and N07, where Q was increased from 0 to 2.24 with a constant ε of 19%. Contraction and double twins were not observed in Fig. 6 (c), but they were generated with increasing Q (corresponding arrows in Fig. 6 (d)). Double twins were observed within the contraction twins. This phenomenon is consistent with previous reports (Ion et al., 1982; L. Jiang et al., 2007). In Fig. 6 (b) (c) and (d), the ε was approximately 19%, some of grains had almost half of their area occupied by well-developed extension twins (see white arrows in Fig. 6), and the intersection of twins can be observed for high levels of ε .

4. Discussion

4.1. Twinning development during cold-rolling

During cold rolling, $\langle c + a \rangle$ slip was suppressed, while twinning was generally favoured. Therefore, twinning played an important role during fabrication of the Mg tubes. Texture development and reorientations of grains are inevitable during deformation of the AZ31 tubes and both extension and contraction twinning may be activated simultaneously (Liang, Sun, Liu, & Wang, 2009; Ranjbar Bahadori, Dehghani, & Bakhshandeh, 2013). The c -axis of the grains tends to rotate into alignment with the deformation direction (Kim et al., 2005; Ma et al., 2012). In the case of increasing ε , there was compressive stress on the RD and TD components (Fig. 4), while extension twins were observed in reoriented grains with their c -axis parallel to the ED due to elongation in this direction (see blue arrows in Fig. 6 (b)). Jiang et al. (L. Jiang et al., 2007) reported that twinning activities were active in the RD component and TD component for extruded tubes. However, extension twinning that occurred in the ED component was observed during cold rolling for the present paper (Fig. 6). Thus, there were grains which were reoriented to the ED component during the cold-rolling of AZ31 tubes.

Contraction twinning remained inactive during the early stages of straining until the local stress reaches the critical resolved shear stress value for contraction (L. Zhang et al., 2013). Therefore, although both the RD component and TD component favour contraction twinning, contraction twins were not observed at an ε of 5.5% (Fig. 6 (a)). In comparison, extension twinning occurred in the ED component more readily than contraction twinning. The extension twins contribute a majority of twins in the case of increasing ε , even at the highest ε of 19.7%. However, it is observed that contraction

twins or double twins also formed for the higher levels of ε (Fig. 6 (c)). Fig. 8 shows pole figures for E1 and E4/Q3, where the ε was increased from 5.5% to 19.7%. Both exhibit a strong overall texture, but the basal planes for those parallel to the ED was enhanced with the increasing ε , caused by tensile stress on the ED and compressive stress on the RD and TD.

As Q was increased, tensile stress and compressive stress was applied on the TD and RD components, respectively (Fig. 4). In comparison with the case of varying ε , no resolved stress was applied along ED. Mechanical twinning in the ED component could not be activated. Extension twins were broadly distributed in all samples of Q groups, which resulted from the high-level ε of 19.7%. However, limited extension twins propagated in the TD. Referring to the Schmid Factor (SF) criterion, only those twin variants above a threshold value of SF can form during deformation (Mu, Jonas, & Gottstein, 2012; Park, Hong, Lee, & Lee, 2012). The resolved stress in the case of those samples with varying Q is similar to the condition of tests conducted by Godet et al. (Godet, Jiang, Luo, & Jonas, 2006), where contraction twins were shown to have a higher SF than that of extension twins. Therefore, contraction twins developed rapidly with an increase in Q . Much more contraction twins formed than extension twins as shown in Fig. 6 (d). As mentioned above, texture intensity near the TD component became lower for the higher level of ε . This may also contribute to the suppression of extension twinning in the case of varying Q (ε remained at approximately 19%) due to the lack of an appropriate component for twinning. Jiang et al. (L. Jiang et al., 2007) analysed a similar condition, and concluded that the RD component was rotated more readily towards ED than towards the TD component using the SF criterion, which is consistent with the above result.

4.2. Influence of twinning on mechanical behaviour

The influence of twinning on the mechanical behaviour of Mg alloys has been demonstrated in many studies (Barnett, Keshavarz, Beer, & Atwell, 2004; Barnett, Nave, et al., 2004; Miao, Hu, Wang, & Wang, 2011; Oppedal et al., 2012). The twin boundaries formed in grains can act as barriers to dislocation motion, as do grain boundaries, which can lead to an increase in the work-hardening rate. In contrast, the twin boundaries accommodate strain along the c -axis, which can release the effect of work hardening. Therefore, the lattice rotation introduced by twinning can enhance or reduce the rate of work hardening depending on the type of twinning. $\{10\bar{1}1\}$ contraction twinning reorients the basal planes by 56° and has an effect favourable for basal glide. Double twinning has the same effect as $\{10\bar{1}1\}$ twinning, which rotates the orientation of basal planes by 38° (Lan Jiang et al., 2007). $\{10\bar{1}2\}$ extension twinning reorients the basal planes by 86° (Barnett, Nave, et al., 2004).

In the case of increasing ε , extension twins were generated favourably in the ED direction, and most of the twins in Fig. 6 were identified to be extension ones. Barnett et al. (Barnett, Keshavarz, et al., 2004) pointed out that the 86° reorientation induced by $\{10\bar{1}2\}$ extension twinning has a strong influence on improving strength. Oppedal et al. (Oppedal et al., 2012) reported that extension twinning induces dislocation transformation in the reoriented matrix, as twinning shear extracts from

the parent dislocation and releases a transmuted dislocation in the twin [11, 23]. The increase in strength may also contribute to texture hardening which is verified by Oppedal et al. (Oppedal et al., 2012). Texture hardening took place with increasing ε due to deformation in ED and reorientation of TD component grains. Therefore, the UTS at an ε of 19.7% increased by 33% over that at an ε of 5.5%. Therefore, the combined effect of texture hardening and extension twinning leads to an increase of the UTS and YS in the case of increasing ε .

$\{10\bar{1}1\}$ - $\{10\bar{1}2\}$ double twinning is frequently formed within $\{10\bar{1}1\}$ contraction twins, and has a similar effect on softening to contraction twins (Cizek & Barnett, 2008; Ma et al., 2012). However, this type of structure is considered to lead to rapid flow localisation and failure (Cizek & Barnett, 2008) due to the combined effects of strain softening and localised void formation (Barnett, 2007). In both cases of increasing ε and increasing Q , the elongations declined. For the case of increasing ε , texture hardening and extension twinning may be factors which lead to the drop in elongation, so the effect of double twins on elongation could not be ascertained. But with increasing Q , elongation experienced a decreasing trend similar to UTS and YS, which is not consistent with typical mechanical behaviours. In consideration of the absence of texture hardening and the unchanged amount of extension twins, the effect of double twins may contribute to this seemingly abnormal tendency. Fig. 9 shows pole figures of the grain orientations for N02 and N07 (Q increased from 0 to 2.24). The texture was not enhanced along any particular direction.

The apparent fraction of twins in samples with high ε levels seemed lower because most of the grains have been almost entirely consumed and reoriented by twinning. These conditions favour the activation of secondary $\{10\bar{1}2\}$ twinning for all with increasing Q (Cizek & Barnett, 2008). In the case of increasing ε , secondary $\{10\bar{1}2\}$ twinning was observed in the sample with ε of 19.7% (Fig. 6 (b) & (d)). The frequency of the secondary twin boundaries increases continuously with strain. More and more secondary twinning can be activated within primary $\{10\bar{1}2\}$ twins. Unlike most of the primary $\{10\bar{1}2\}$ twins, these secondary $\{10\bar{1}2\}$ twins were shorter and denser (Cizek & Barnett, 2008; Lan Jiang et al., 2007). That is because secondary twins have a high rate of lateral growth, and then consume significant lengths of the primary twins. The secondary $\{10\bar{1}2\}$ twins were observed in the samples processed at a Q of 2.24 (arrows in Fig. 6 (d)). As mentioned earlier, twin boundaries can have the effect of blocking dislocation motion. The primary $\{10\bar{1}2\}$ twins provide additional barriers to the secondary $\{10\bar{1}2\}$ twin systems. Hence, the formation of primary and secondary $\{10\bar{1}2\}$ twins contribute to hardening. However, Jiang et al. (Lan Jiang et al., 2007) reported a decrease in the strain hardening rate when primary and secondary $\{10\bar{1}2\}$ twin systems interacted, which is also observed in the results of this investigation. The reason for this behaviour is unclear and requires further research.

Texture in the ED did not change with varying Q . As deformation took place in the TD and RD, the UTS and YS exhibited a rapid drop with increasing Q , which suggests that the change of texture in TD and RD does not play as important a role as that in the case of varying ε . However, the formation of $\{10\bar{1}1\}$ contraction twinning had a significant influence on the flow stress. Its effect was reported to be similar to that of $\langle c + a \rangle$ slip [32]. It is observed that $\{10\bar{1}1\}$ contraction twinning and double twinning can be activated in the RD (Fig. 4), and they increased linearly with the increase of Q . Decreasing strain hardening resulted from the formation of contraction and double twins due to the reduction of the strain hardening index, n (Jiang, Jonas, Luo, Sachdev, & Godet, 2006). Extension

twinning may also be activated in the TD. However, as mentioned earlier, many of the grains have been almost completely consumed and reoriented by twinning at an ε of 19.7%, so extension twinning was suppressed even when Q is 0. The amount of primary $\{10\bar{1}2\}$ twins rarely increased because they were almost saturated, while the shorter and denser secondary $\{10\bar{1}2\}$ twins are introduced. The twins lost their effectiveness as barriers to dislocation motion. This contributes to the decrease in strain hardening rate observed in Fig. 3 with increasing Q . Therefore, in the case of increasing Q , primary $\{10\bar{1}2\}$ extension twinning has no influence on the mechanical behaviour, while the combined effects of $\{10\bar{1}1\}$ twinning/double twinning and secondary $\{10\bar{1}2\}$ twinning play a dominant role.

Accepted manuscript

5. Conclusion

The effect of cold rolling on the mechanical behaviour of AZ31 Mg alloy tubes was investigated through an analysis of mechanical properties and the evolution of twinning under different processing parameters. The properties were assessed with respect to the tube rolling parameters; ε the ratio in cross-sectional reduction and Q the ratio of wall-thickness to diameter reduction.

For the AZ31 tubes, the UTS and YS increased with increasing ε , while it dropped with an increase in Q . Elongation in both cases decreased with an increase in ε and Q . The UTS/YS and elongation show the same tendency due to the formation of $\{10\bar{1}1\}$ - $\{10\bar{1}2\}$ double twins.

$\{10\bar{1}2\}$ extension twins increased with increasing ε until they are almost saturated when ε is above 16.5%. Then contraction/double twins and secondary $\{10\bar{1}2\}$ twins propagated dramatically at high-levels ($\geq 16.5\%$) of ε and in the case of increasing Q .

The $\{10\bar{1}2\}$ extension twins were the dominant deformation mechanism and overshadowed that of contraction and double twinning in the case of varying ε . Texture hardening and $\{10\bar{1}2\}$ extension twinning are the two dominant effects on the mechanical properties in the case of increasing ε . Contraction and double twinning played a dominant role in determining the mechanical behaviour in the case of varying Q .

Acknowledgement

The authors would like to acknowledge the support of the Queensland Centre for Advanced Materials Processing and Manufacturing (AMPAM), and China Scholarship Council for the scholarship support.

References

- Al-Samman, T., Molodov, K. D., Molodov, D. A., Gottstein, G., & Suwas, S. (2012). Softening and dynamic recrystallization in magnesium single crystals during c-axis compression. *Acta Materialia*, *60*(2), 537-545. doi: <http://dx.doi.org/10.1016/j.actamat.2011.10.013>
- ASTM. (2013). Standard Test Methods for Determining Average Grain Size. West Conshohocken, PA.
- Ball, E. A., & Prangnell, P. B. (1994). Tensile-compressive yield asymmetries in high strength wrought magnesium alloys. *Scripta Metallurgica et Materialia*, *31*(2), 111-116.
- Barnett, M. R. (2001). Influence of deformation conditions and texture on the high temperature flow stress of magnesium AZ31. *Journal of Light Metals*, *1*(3), 167-177. doi: [http://dx.doi.org/10.1016/S1471-5317\(01\)00010-4](http://dx.doi.org/10.1016/S1471-5317(01)00010-4)
- Barnett, M. R. (2007). Twinning and the ductility of magnesium alloys: Part II. "Contraction" twins. *Materials Science and Engineering: A*, *464*(1-2), 8-16. doi: <http://dx.doi.org/10.1016/j.msea.2007.02.109>
- Barnett, M. R., Keshavarz, Z., Beer, A. G., & Atwell, D. (2004). Influence of grain size on the compressive deformation of wrought Mg-3Al-1Zn. *Acta Materialia*, *52*(17), 5093-5103. doi: <http://dx.doi.org/10.1016/j.actamat.2004.07.015>
- Barnett, M. R., Nave, M. D., & Bettles, C. J. (2004). Deformation microstructures and textures of some cold rolled Mg alloys. *Materials Science and Engineering: A*, *386*(1-2), 205-211. doi: <http://dx.doi.org/10.1016/j.msea.2004.07.030>
- Bohlen, J., Dobron, P., Garcia, E. M., Chmelík, F., Lukáč, P., Letzig, D., & Kainer, K. U. (2006). The effect of grain size on the deformation behaviour of magnesium alloys investigated by the acoustic emission technique. *Advanced Engineering Materials*, *8*(5), 422-427.
- Chao, H.-y., Sun, H.-f., & Wang, E.-d. (2011). Working hardening behaviors of severely cold deformed and fine-grained AZ31 Mg alloys at room temperature. *Transactions of Nonferrous Metals Society of China*, *21*, Supplement 2(0), s235-s241. doi: [http://dx.doi.org/10.1016/S1003-6326\(11\)61584-7](http://dx.doi.org/10.1016/S1003-6326(11)61584-7)
- Chen, F.-K., & Huang, T.-B. (2003). Formability of stamping magnesium-alloy AZ31 sheets. *Journal of Materials Processing Technology*, *142*(3), 643-647. doi: [http://dx.doi.org/10.1016/S0924-0136\(03\)00684-8](http://dx.doi.org/10.1016/S0924-0136(03)00684-8)
- Chino, Y., Hoshika, T., Lee, J.-S., & Mabuchi, M. (2006). Mechanical properties of AZ31 Mg alloy recycled by severe deformation. *Journal of Materials Research*, *21*(03), 754-760. doi: [doi:10.1557/jmr.2006.0090](https://doi.org/10.1557/jmr.2006.0090)
- Chino, Y., Kimura, K., & Mabuchi, M. (2008). Twinning behavior and deformation mechanisms of extruded AZ31 Mg alloy. *Materials Science and Engineering: A*, *486*(1-2), 481-488. doi: <http://dx.doi.org/10.1016/j.msea.2007.09.058>
- Cizek, P., & Barnett, M. R. (2008). Characteristics of the contraction twins formed close to the fracture surface in Mg-3Al-1Zn alloy deformed in tension. *Scripta Materialia*, *59*(9), 959-962. doi: <http://dx.doi.org/10.1016/j.scriptamat.2008.06.041>
- del Valle, J. A., Carreño, F., & Ruano, O. A. (2006). Influence of texture and grain size on work hardening and ductility in magnesium-based alloys processed by ECAP and rolling. *Acta Materialia*, *54*(16), 4247-4259. doi: <http://dx.doi.org/10.1016/j.actamat.2006.05.018>
- Erbel, R., Di Mario, C., Bartunek, J., Bonnier, J., de Bruyne, B., Eberli, F. R., . . . Waksman, R. Temporary scaffolding of coronary arteries with bioabsorbable magnesium stents: a prospective, non-randomised multicentre trial. *The Lancet*, *369*(9576), 1869-1875. doi: [http://dx.doi.org/10.1016/S0140-6736\(07\)60853-8](http://dx.doi.org/10.1016/S0140-6736(07)60853-8)
- Farrar, G., Blair, J. A., Altmann, P., & Welch, S. (1990). Comparative plasma speciation of the aluminium model 'gallium-67' in Alzheimers disease, stroke dementia, downs syndrome, end-stage renal disease and controls. *Neurobiology of Aging*, *11*(3), 318. doi: [http://dx.doi.org/10.1016/0197-4580\(90\)90822-H](http://dx.doi.org/10.1016/0197-4580(90)90822-H)

- Gharghoury, M. A., Weatherly, G. C., Embury, J. D., & Root, J. (1999). Study of the mechanical properties of Mg-7.7at.% Al by in-situ neutron diffraction. *Philosophical Magazine A: Physics of Condensed Matter, Structure, Defects and Mechanical Properties*, 79(7), 1671-1695.
- Godet, S., Jiang, L., Luo, A. A., & Jonas, J. J. (2006). Use of Schmid factors to select extension twin variants in extruded magnesium alloy tubes. *Scripta Materialia*, 55(11), 1055-1058. doi: <http://dx.doi.org/10.1016/j.scriptamat.2006.07.059>
- Guan, L., Tang, G., Jiang, Y., & Chu, P. K. (2009). Texture evolution in cold-rolled AZ31 magnesium alloy during electropulsing treatment. *Journal of Alloys and Compounds*, 487(1-2), 309-313. doi: <http://dx.doi.org/10.1016/j.jallcom.2009.07.114>
- Hanada, K., Matsuzaki, K., Huang, X., & Chino, Y. (2013). Fabrication of Mg alloy tubes for biodegradable stent application. *Materials Science and Engineering: C*, 33(8), 4746-4750. doi: <http://dx.doi.org/10.1016/j.msec.2013.07.033>
- Hermawan, H., Dubé, D., & Mantovani, D. (2010). Developments in metallic biodegradable stents. *Acta Biomaterialia*, 6(5), 1693-1697. doi: 10.1016/j.actbio.2009.10.006
- Heublein, B., Rohde, R., Kaese, V., Niemeyer, M., Hartung, W., & Haverich, A. (2003). Biocorrosion of magnesium alloys: A new principle in cardiovascular implant technology? *Heart*, 89(6), 651-656.
- Hu, J., Zhang, C., Cui, B., Bai, K., Guan, S., Wang, L., & Zhu, S. (2011). In vitro degradation of AZ31 magnesium alloy coated with nano TiO₂ film by sol-gel method. *Applied Surface Science*, 257(21), 8772-8777. doi: <http://dx.doi.org/10.1016/j.apsusc.2011.03.148>
- Huber, J., & Hatherly, M. (1980). NUCLEATION AND ANNEALING TEXTURE DEVELOPMENT IN ROLLED 70:30 BRASS. *Zeitschrift fuer Metallkunde/Materials Research and Advanced Techniques*, 71(1), 15-20.
- Ion, S. E., Humphreys, F. J., & White, S. H. (1982). Dynamic recrystallisation and the development of microstructure during the high temperature deformation of magnesium. *Acta Metallurgica*, 30(10), 1909-1919. doi: [http://dx.doi.org/10.1016/0001-6160\(82\)90031-1](http://dx.doi.org/10.1016/0001-6160(82)90031-1)
- Jiang, L., Jonas, J. J., Luo, A. A., Sachdev, A. K., & Godet, S. (2006). Twinning-induced softening in polycrystalline AM30 Mg alloy at moderate temperatures. *Scripta Materialia*, 54(5), 771-775. doi: <http://dx.doi.org/10.1016/j.scriptamat.2005.11.029>
- Jiang, L., Jonas, J. J., Luo, A. A., Sachdev, A. K., & Godet, S. (2007). Influence of {10-12} extension twinning on the flow behavior of AZ31 Mg alloy. *Materials Science and Engineering: A*, 445-446(0), 302-309. doi: <http://dx.doi.org/10.1016/j.msea.2006.09.069>
- Jiang, L., Jonas, J. J., Mishra, R. K., Luo, A. A., Sachdev, A. K., & Godet, S. (2007). Twinning and texture development in two Mg alloys subjected to loading along three different strain paths. *Acta Materialia*, 55(11), 3899-3910. doi: <http://dx.doi.org/10.1016/j.actamat.2007.03.006>
- Jonas, J. J., Mu, S., Al-Samman, T., Gottstein, G., Jiang, L., & Martin, E. (2011). The role of strain accommodation during the variant selection of primary twins in magnesium. *Acta Materialia*, 59(5), 2046-2056.
- Kim, S.-H., You, B.-S., Dong Yim, C., & Seo, Y.-M. (2005). Texture and microstructure changes in asymmetrically hot rolled AZ31 magnesium alloy sheets. *Materials Letters*, 59(29-30), 3876-3880. doi: <http://dx.doi.org/10.1016/j.matlet.2005.07.024>
- Knezevic, M., Levinson, A., Harris, R., Mishra, R. K., Doherty, R. D., & Kalidindi, S. R. (2010). Deformation twinning in AZ31: Influence on strain hardening and texture evolution. *Acta Materialia*, 58(19), 6230-6242. doi: <http://dx.doi.org/10.1016/j.actamat.2010.07.041>
- Koike, J. (2005). Enhanced deformation mechanisms by anisotropic plasticity in polycrystalline Mg alloys at room temperature. *Metallurgical and Materials Transactions A: Physical Metallurgy and Materials Science*, 36(7), 1689-1696.
- Koike, J., & Ohyama, R. (2005). Geometrical criterion for the activation of prismatic slip in AZ61 Mg alloy sheets deformed at room temperature. *Acta Materialia*, 53(7), 1963-1972. doi: <http://dx.doi.org/10.1016/j.actamat.2005.01.008>

- Lévesque, J., Hermawan, H., Dubé, D., & Mantovani, D. (2008). Design of a pseudo-physiological test bench specific to the development of biodegradable metallic biomaterials. *Acta Biomaterialia*, 4(2), 284-295.
- Liang, S., Sun, H., Liu, Z., & Wang, E. (2009). Mechanical properties and texture evolution during rolling process of an AZ31 Mg alloy. *Journal of Alloys and Compounds*, 472(1–2), 127-132. doi: <http://dx.doi.org/10.1016/j.jallcom.2008.04.093>
- Liu, X., Jonas, J. J., Li, L. X., & Zhu, B. W. (2013). Flow softening, twinning and dynamic recrystallization in AZ31 magnesium. *Materials Science and Engineering: A*, 583(0), 242-253. doi: <http://dx.doi.org/10.1016/j.msea.2013.06.074>
- Ma, Q., El Kadiri, H., Oppedal, A. L., Baird, J. C., Li, B., Horstemeyer, M. F., & Vogel, S. C. (2012). Twinning effects in a rod-textured AM30 Magnesium alloy. *International Journal of Plasticity*, 29(0), 60-76. doi: <http://dx.doi.org/10.1016/j.ijplas.2011.08.001>
- Meza-García, E., Dobroň, P., Bohlen, J., Letzig, D., Chmelík, F., Lukáč, P., & Kainer, K. U. (2007). Deformation mechanisms in an AZ31 cast magnesium alloy as investigated by the acoustic emission technique. *Materials Science and Engineering A*, 462(1-2), 297-301.
- Miao, Q., Hu, L., Wang, G., & Wang, E. (2011). Fabrication of excellent mechanical properties AZ31 magnesium alloy sheets by conventional rolling and subsequent annealing. *Materials Science and Engineering: A*, 528(22–23), 6694-6701. doi: <http://dx.doi.org/10.1016/j.msea.2011.05.023>
- Mu, S., Jonas, J. J., & Gottstein, G. (2012). Variant selection of primary, secondary and tertiary twins in a deformed Mg alloy. *Acta Materialia*, 60(5), 2043-2053. doi: <http://dx.doi.org/10.1016/j.actamat.2012.01.014>
- Myshlyaev, M. M., McQueen, H. J., Mwembela, A., & Konopleva, E. (2002). Twinning, dynamic recovery and recrystallization in hot worked Mg-Al-Zn alloy. *Materials Science and Engineering A*, 337(1-2), 121-133.
- Oppedal, A. L., El Kadiri, H., Tomé, C. N., Kaschner, G. C., Vogel, S. C., Baird, J. C., & Horstemeyer, M. F. (2012). Effect of dislocation transmutation on modeling hardening mechanisms by twinning in magnesium. *International Journal of Plasticity*, 30–31(0), 41-61. doi: <http://dx.doi.org/10.1016/j.ijplas.2011.09.002>
- Park, S. H., Hong, S.-G., Lee, J. H., & Lee, C. S. (2012). Multiple twinning modes in rolled Mg–3Al–1Zn alloy and their selection mechanism. *Materials Science and Engineering: A*, 532(0), 401-406. doi: <http://dx.doi.org/10.1016/j.msea.2011.11.003>
- Phillipson, M. (1988). The link between aluminium and Alzheimers—Not the whole story. *Food and Chemical Toxicology*, 26(1), 76-77. doi: [http://dx.doi.org/10.1016/0278-6915\(88\)90047-6](http://dx.doi.org/10.1016/0278-6915(88)90047-6)
- Ranjbar Bahadori, S., Dehghani, K., & Bakhshandeh, F. (2013). Microstructure, texture and mechanical properties of pure copper processed by ECAP and subsequent cold rolling. *Materials Science and Engineering: A*, 583(0), 36-42. doi: <http://dx.doi.org/10.1016/j.msea.2013.06.061>
- Rohatgi, A., Vecchio, K. S., & Gray, I. G. T. (2001). A metallographic and quantitative analysis of the influence of stacking fault energy on shock-hardening in Cu and Cu–Al alloys. *Acta Materialia*, 49(3), 427-438. doi: [http://dx.doi.org/10.1016/S1359-6454\(00\)00335-9](http://dx.doi.org/10.1016/S1359-6454(00)00335-9)
- Styczynski, A., Hartig, C., Bohlen, J., & Letzig, D. (2004). Cold rolling textures in AZ31 wrought magnesium alloy. *Scripta Materialia*, 50(7), 943-947. doi: <http://dx.doi.org/10.1016/j.scriptamat.2004.01.010>
- Tenckhoff, E. (1988). *Deformation Mechanisms, Texture, and Anisotropy in Zirconium and Zircaloy*.
- Wang, Y. N., & Huang, J. C. (2007). The role of twinning and untwinning in yielding behavior in hot-extruded Mg-Al-Zn alloy. *Acta Materialia*, 55(3), 897-905.
- Yang, L.-f., Mori, K.-i., & Tsuji, H. (2008). Deformation behaviors of magnesium alloy AZ31 sheet in cold deep drawing. *Transactions of Nonferrous Metals Society of China*, 18(1), 86-91. doi: [http://dx.doi.org/10.1016/S1003-6326\(08\)60016-3](http://dx.doi.org/10.1016/S1003-6326(08)60016-3)

- Yang, X., Okabe, Y., Miura, H., & Sakai, T. (2012). Effect of pass strain and temperature on recrystallisation in magnesium alloy AZ31 after interrupted cold deformation. *Journal of Materials Science*, 47(6), 2823-2830. doi: 10.1007/s10853-011-6111-6
- Yoo, M. H. (1981). Slip, twinning, and fracture in hexagonal close-packed metals. *Metallurgical Transactions A*, 12(3), 409-418.
- Zeng, R.-C., Hu, Y., Guan, S.-K., Cui, H.-Z., & Han, E.-H. Corrosion of magnesium alloy AZ31: The influence of bicarbonate, sulphate, hydrogen phosphate and dihydrogen phosphate ions in saline solution. *Corrosion Science*(0). doi: <http://dx.doi.org/10.1016/j.corsci.2014.05.006>
- Zhang, L., Liu, C.-G., Wang, H.-Y., Nan, X.-L., Xiao, W., & Jiang, Q.-C. (2013). Twinning and mechanical behavior of an extruded Mg–6Al–3Sn alloy with a dual basal texture. *Materials Science and Engineering: A*, 578(0), 14-17. doi: <http://dx.doi.org/10.1016/j.msea.2013.04.026>
- Zhang, Z., Rauch, E. F., & Véron, M. (2013). Twinning analyses in a magnesium alloy with tilting series scanning method using a TEM based orientation mapping system. *Materials Letters*, 111(0), 192-196. doi: <http://dx.doi.org/10.1016/j.matlet.2013.08.072>
- Zomorodian, A., Garcia, M. P., Moura e Silva, T., Fernandes, J. C. S., Fernandes, M. H., & Montemor, M. F. (2013). Corrosion resistance of a composite polymeric coating applied on biodegradable AZ31 magnesium alloy. *Acta Biomaterialia*, 9(10), 8660-8670. doi: <http://dx.doi.org/10.1016/j.actbio.2013.02.036>
- Zong, Y., Yuan, G., Zhang, X., Mao, L., Niu, J., & Ding, W. (2012). Comparison of biodegradable behaviors of AZ31 and Mg–Nd–Zn–Zr alloys in Hank's physiological solution. *Materials Science and Engineering: B*, 177(5), 395-401. doi: <http://dx.doi.org/10.1016/j.mseb.2011.09.042>

Tables:

Table.1 Chemical composition of the AZ31B tubes (wt. %).

Mg	Al	Zn	Mn	Cu	Fe	Ni
Balance	2.70	0.71	0.20	0.008	0.007	0.001

Table. 2 Sample groups and processing parameters ε and Q used in investigation.

Sample	E1	E2	E3	E4/Q3	Q1	Q2	E4/Q3	Q4
Outside Diameter (mm)	7.71	7.51	7.32	7.19	6.57	6.91	7.19	7.41
Wall thickness (mm)	0.87	0.84	0.81	0.79	0.90	0.84	0.79	0.77
ε	5.5%	11.1%	16.3%	19.7%	Approximately 19%			
Q	1.37				0	0.53	1.37	2.24

Table. 3. Statistical grain sizes with Q of 1.37

	ε of 5.5%	ε of 11.1%	ε of 16.5%	ε of 19.7%
Grain sizes	17.64 μm	17.51 μm	17.81 μm	18.17 μm

Figures:

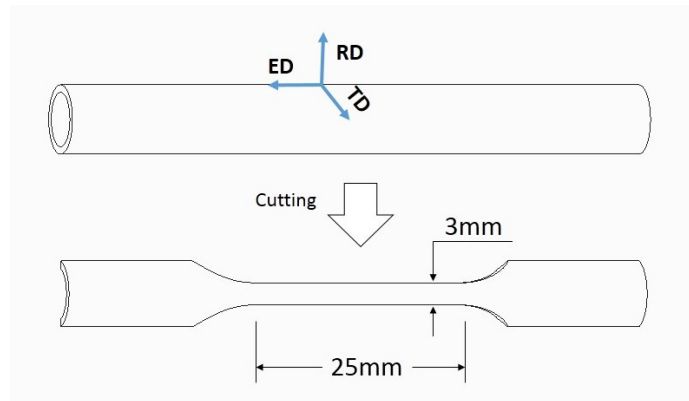


Fig.1 Schematic diagram relating the elongation direction (ED), tangential direction (TD) and radial direction (RD) to the sample orientation.

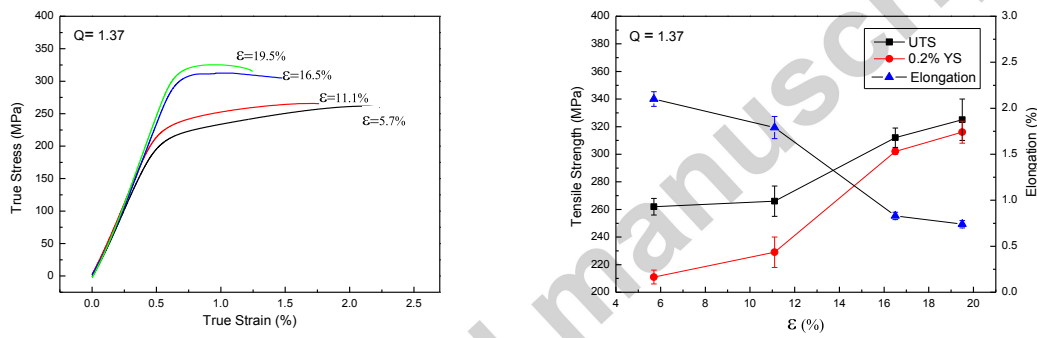


Fig. 2 (a) True stress-true strain plots for varying ϵ ; (b) Evolution of mechanical properties with ϵ (Standard error bars)

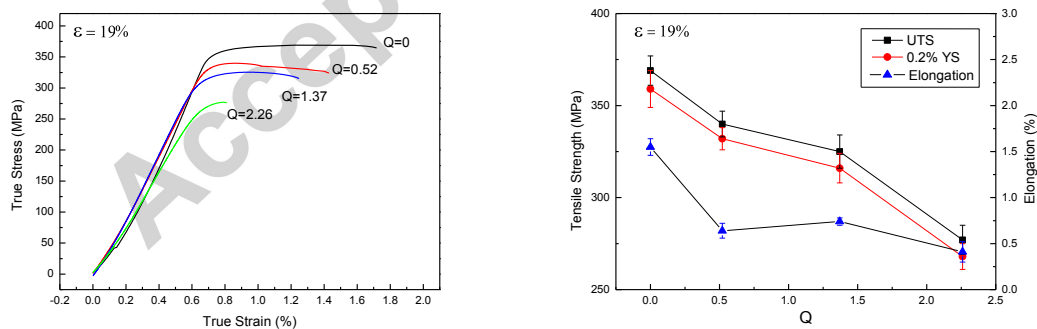


Fig. 3 (a) True stress-true strain behaviour with varying Q ; (b) Evolution of mechanical properties with Q (Standard error bars)

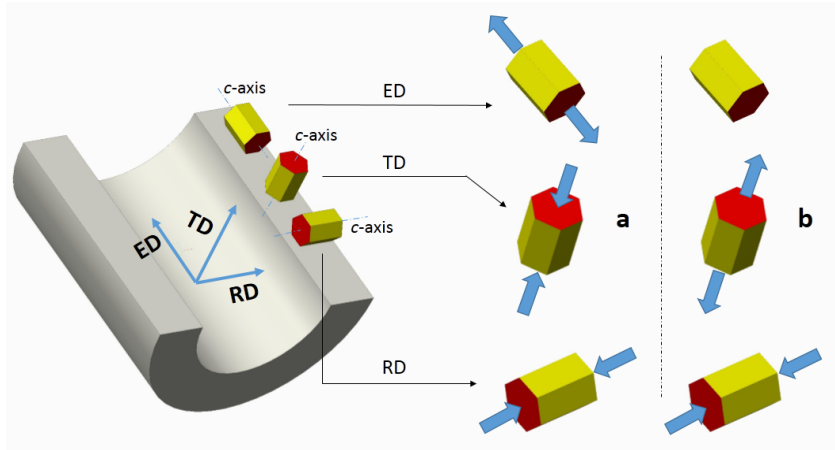


Fig. 4. Schematic diagram relating the orientation of c-axes and resolved stresses on crystals with HCP structure in different directions. (a) resolved stresses as ϵ increases; (b) resolved stresses as Q increases

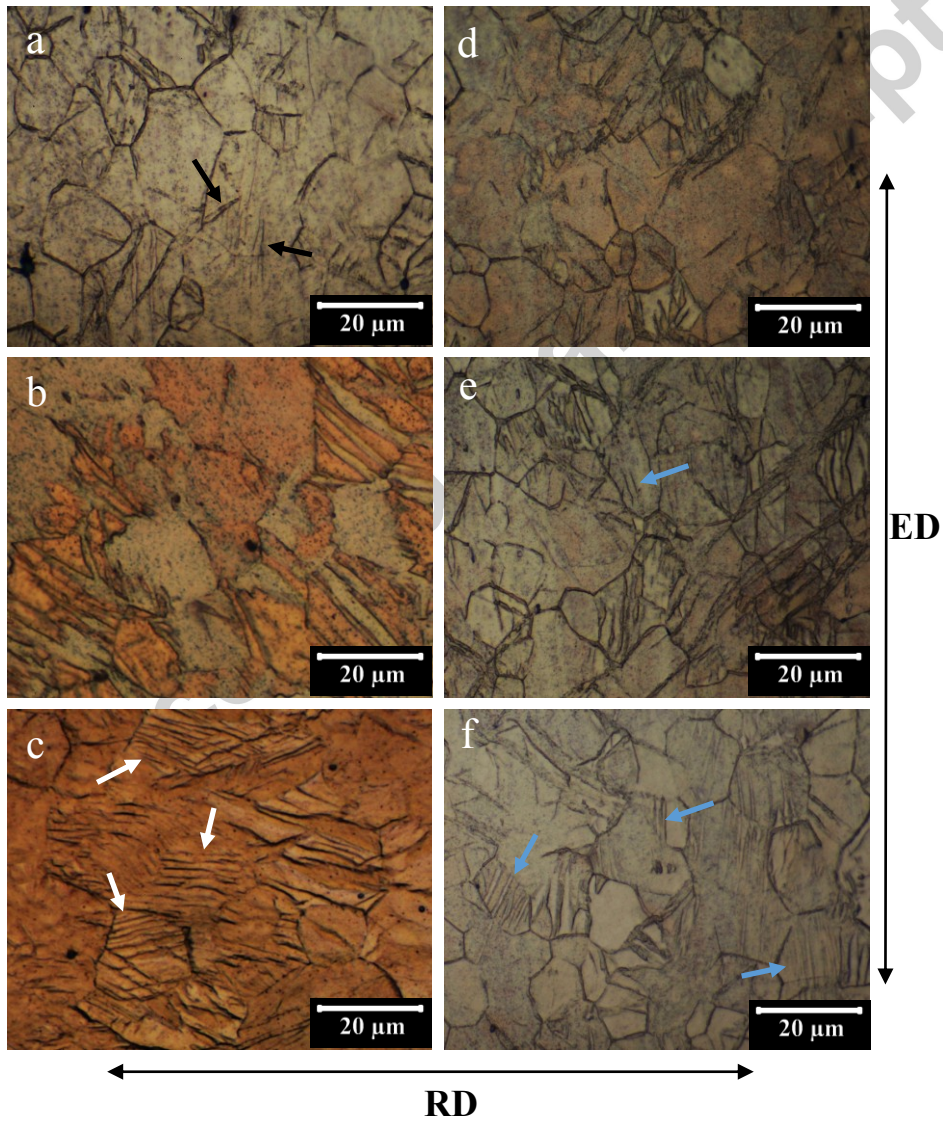


Fig. 5. Microstructures of cold-rolled AZ31 tubes: (a) ϵ : 5.5%, Q : 1.37 (b) ϵ : 16.5%, Q : 1.37 (c) ϵ : 19.7%, Q : 1.37 (d) ϵ : 19.7%, Q : 0, (e) ϵ : 19.7%, Q : 0.53, (f) ϵ : 19.7%, Q : 2.24

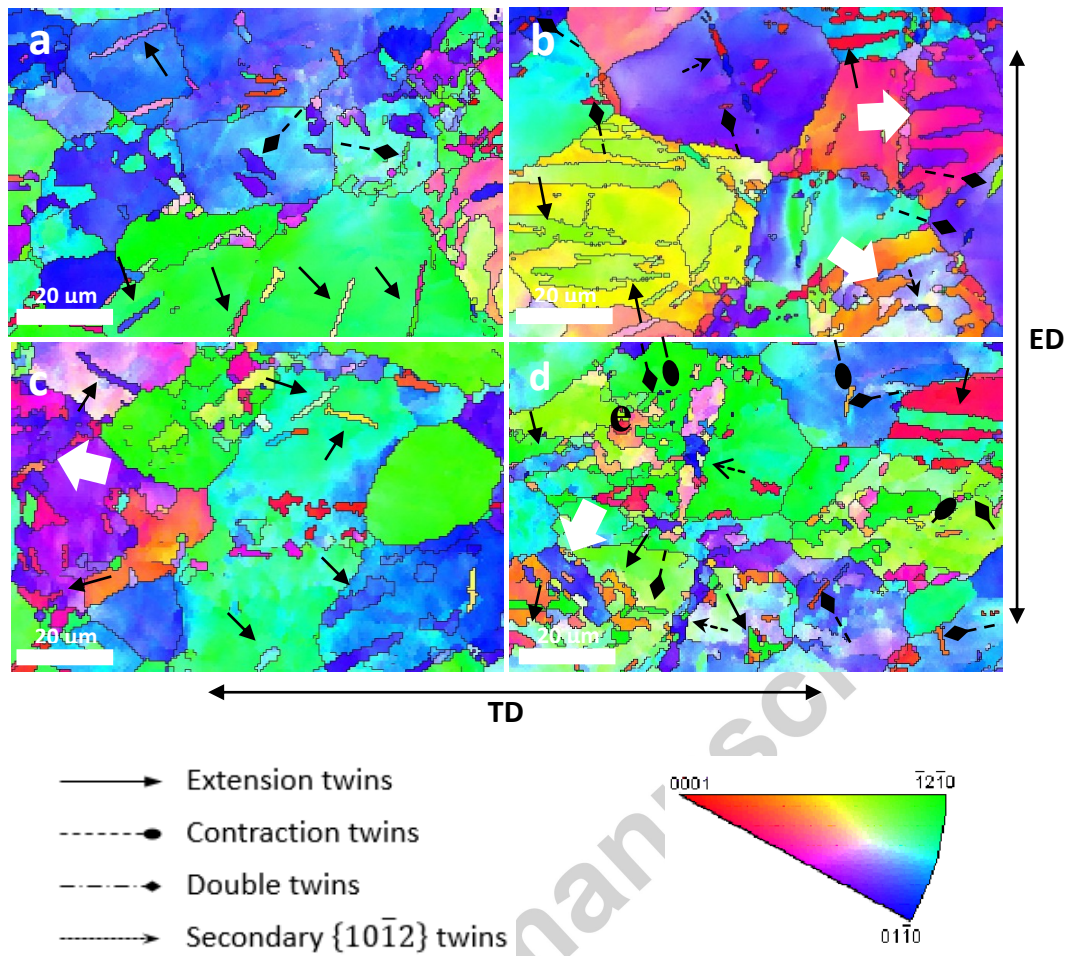


Fig. 6. Inverse pole figure maps obtained by EBSD serial image analyses showing extension twins, contraction twins and double twins in AZ31 magnesium tubes deformed at different ε and Q . (a) ε : 5.5%, Q : 1.37; (b) ε : 19.7%, Q : 1.37; (c) ε : 19.7%, Q : 0; (d) ε : 19.7%, Q : 2.24. The IPF maps correspond to the orientation with respect to the map key in (e).

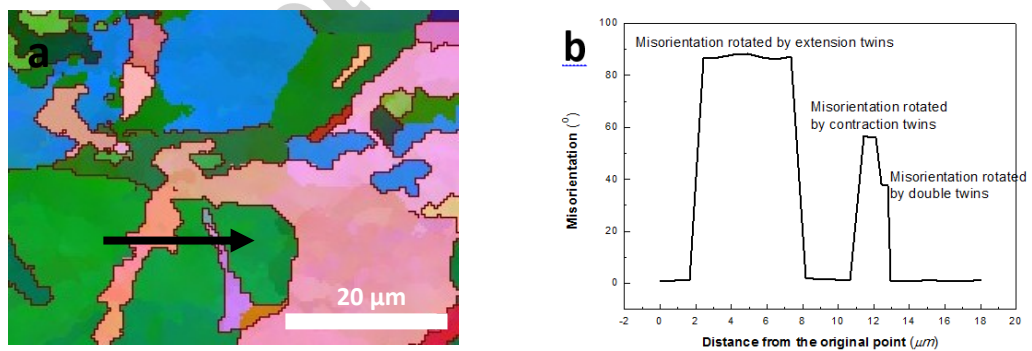


Fig. 7. Schematic diagram for identifying different types of twins by characteristic reorientation angles. (a) Inverse pole figure of the sample with ε of 19.7% and Q of 2.24, reorientation angles were detected along with the black arrow. (b) Misorientation angles for specific twins, extension twins ($87^\circ \pm 3^\circ$), contraction twins ($56^\circ \pm 3^\circ$) and double twins ($37^\circ \pm 3^\circ$) were detected, respectively

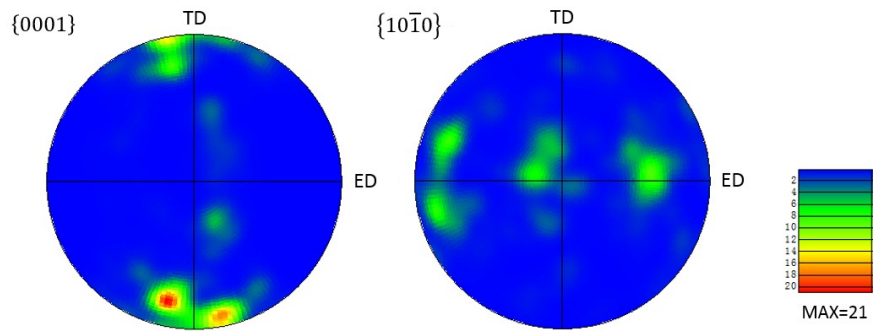
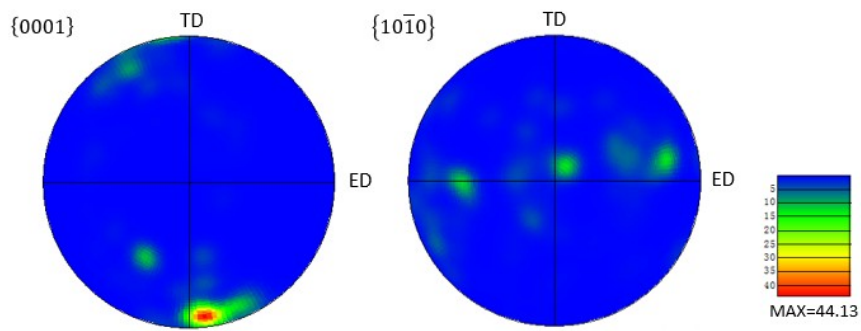
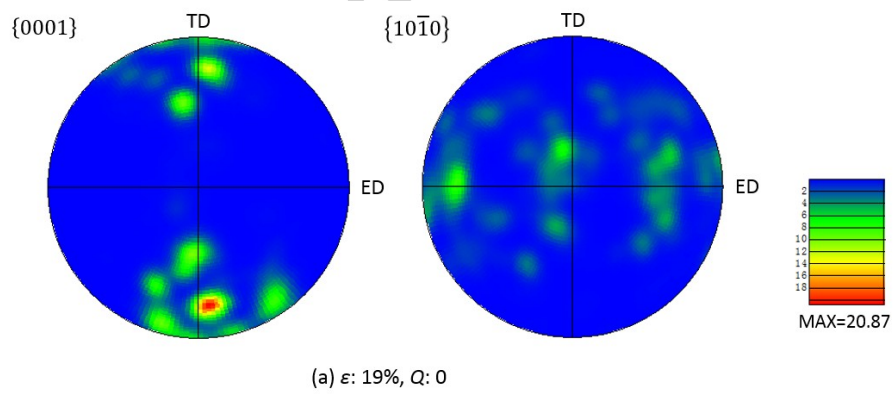
(a) ε : 5.5%, Q : 1.37(b) ε : 19.7%, Q : 1.37

Fig. 8. Texture development during rolling of AZ31 tubes with the increasing Q . Recalculated $\{0001\}$ and $\{10\bar{1}0\}$ pole figures (a) ε : 5.5%, Q : 1.37 (b) ε : 19.7%, Q : 1.37

(a) ε : 19%, Q : 0

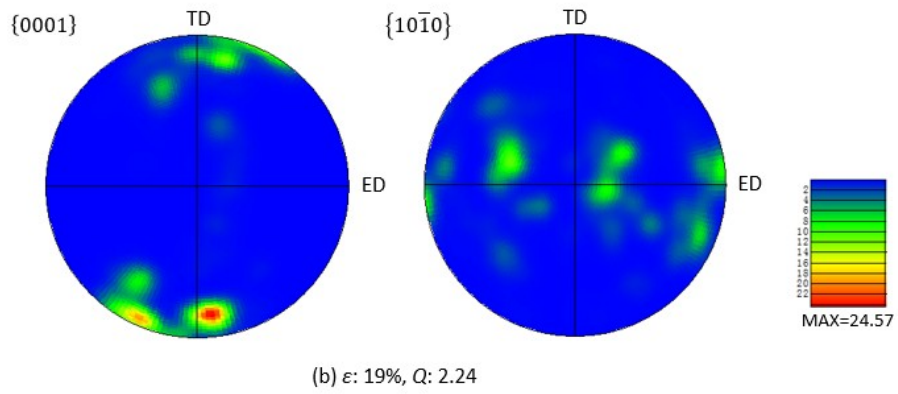


Fig. 9. Texture development during rolling of AZ31 tubes with the increasing Q . Recalculated $\{0001\}$ and $\{10\bar{1}0\}$ pole figures (a) ϵ : 19%, Q : 0 (b) ϵ : 19%, Q : 2.24

Accepted manuscript